Equilibrium calculations of viscosity and thermal conductivity across a solid–liquid interface using boundary fluctuations

ARTICLE *in* THE JOURNAL OF CHEMICAL PHYSICS · JUNE 2008

Impact Factor: 2.95 · DOI: 10.1063/1.2911924 · Source: PubMed

2 AUTHORS, INCLUDING:

Janka Petravic
University of New South Wales
77 PUBLICATIONS **733** CITATIONS

Equilibrium calculations of viscosity and thermal conductivity across a solid-liquid interface using boundary fluctuations

Janka Petravic and Peter Harrowell[a)]
School of Chemistry, The University of Sydney, Sydney, NSW 2006, Australia

(Received 31 December 2007; accepted 27 March 2008; published online 19 May 2008)

We calculate viscosity and thermal conductivity in systems of Lennard–Jones particles consisting of coexisting solid and liquid with different interface wetting properties using the recently developed equilibrium boundary fluctuation theory. We compare the slip length and equivalent liquid length obtained from these calculations with those obtained from nonequilibrium molecular dynamics. The equilibrium and nonequilibrium calculations of the slip length and the sum of the thermal equivalent lengths are in good agreement. We conclude that for both interfacial properties, the nonequilibrium simulations were probing the linear response. The significant dependence of the intrinsic equivalence length on the interfacial temperature difference used to generate the thermal gradient is explained as a consequence of the different thermodynamic states of the two interfaces. © *2008 American Institute of Physics*. [DOI: 10.1063/1.2911924]

I. INTRODUCTION

In this work we calculate the transport coefficients for shear and heat flow across solid-liquid systems containing interfaces with different wetting properties, using the recently developed boundary fluctuation theory (BFT). We compare the equilibrium results to the results of nonequilibrium simulations with two aims in mind. The first is to validate the results of our method, which has so far been applied only to uniform confined systems. The second is to estimate the gradient (i.e., shear rate or temperature gradient) dependence of the transport coefficients in the presence of an interface.

Transport of transverse momentum and heat across a solid-liquid interface are fundamental processes of considerable practical significance. Understanding how the factors such as liquid-solid interactions, surface structure, and roughness influence transport across interfaces is important in the technological areas of lubrication, coating and adhesion, flows in porous media, spreading of liquids on solid surfaces, or in cooling and refrigeration when dispersions of nanometer-sized solid particles in liquids ("nanofluids") are used as high thermal conductivity coolants. It is also important in hydrodynamic modeling of flows of colloidal suspensions or slurries, where the average separation of the dispersed particles is small.

Transport of shear stress or heat across interfaces is conventionally expressed in terms of the distance from the interface where the linear velocity or temperature profiles, extrapolated from the two bulk phases, intersect as shown in Fig. 1. This length is called *slip length*[1] for shear flow and *equivalent length*[2] for heat flow in a temperature gradient. When the extent of the liquid is comparable to slip or equivalent liquid length, one can use bulk values of shear viscosity and thermal conductivity in hydrodynamic modeling of such a system but with the changed boundary conditions.[3] If liquid extent is much larger than slip/equivalent liquid length, interface effects can be neglected.

The slip length and equivalent liquid length can be measured to good accuracy using dissipation methods (e.g., drainage force method for slip length and by measuring the absorption and relaxation of pulsed laser light for boundary thermal conductance). The latest drainage force measurements of the glass-water interface[4] show that there is no slip for water on smooth hydrophilic glass and a slip of $\sim 20 \pm 2$ nm for smooth hydrophobic glass. This is in agreement with the theoretical picture where simple Newtonian liquids wetting a smooth surface show no slip,[5–7] while there is a small slip for shear flow past a smooth nonwetting surface.[8] A slip length of this size would be important in flows in less than micrometer-sized channels or, e.g., in modeling flows of dispersions of hydrophobic particles in water with particle separations of the order of 100 nm, which roughly corresponds to 1% volume fraction of spherical particles of 50 nm diameter.

Heat transport across an interface is measured in terms of the thermal boundary conductance or Kapitza conductance[9,10] G_K. It is defined as the ratio of the known (weak) heat flux and temperature difference between two phases linearly extrapolated to the interface. The interface thermal conductance of platinum particles in water[11] measured by pulsed laser light absorption and relaxation was found to be $G_K \approx 130$ MW m^{-2} K^{-1}, while the interface conductance of carbon nanotubes in water[12] is an order of magnitude lower, $G_K \approx 12$ MW m^{-2} K^{-1}. Since the thermal conductivity of water is $\lambda_w = 0.613$ W m^{-1} K^{-1}, the equivalent length $h_L = \lambda_w / G_K$ of water at the platinum interface is just ~ 5 nm, while for the water-carbon nanotube interface it is ~ 50 nm. The decrease of thermal conductivity of carbon nanotube dispersions due to the resistance of the interface to heat flow will be noticeable even at very low volume fraction (less than 0.1%) of dispersed fibers. It explains why the en-

[a)]Electronic mail: peter@chem.usyd.edu.au.

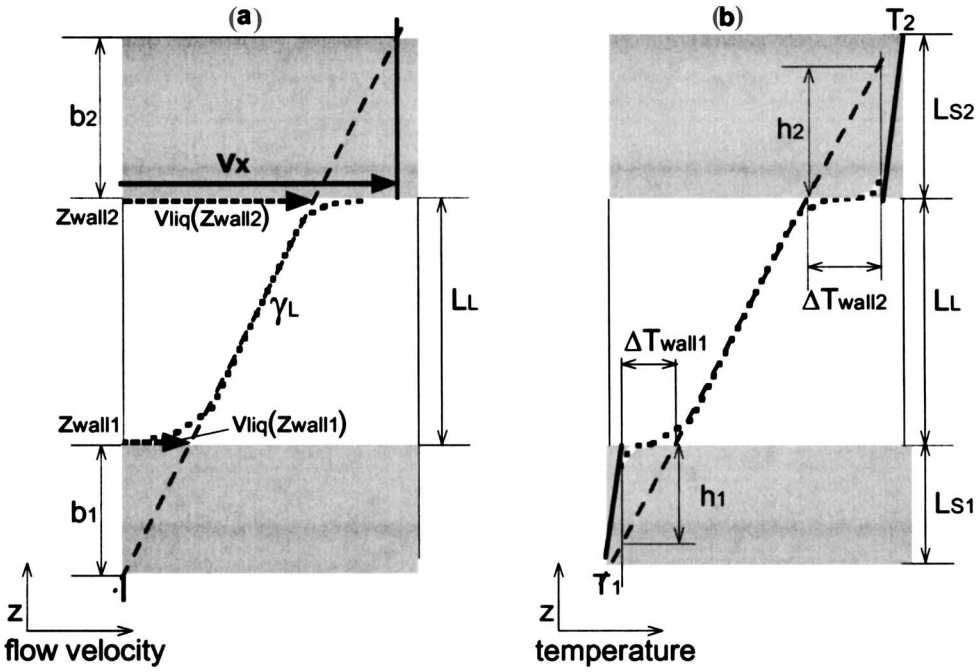

FIG. 1. Flow velocity profile under shear (a) and the temperature profile in the temperature gradient (b) near the solid-liquid interface. Solid is shown in dark gray. (a) The lower wall is at rest, while the upper wall moves with velocity v_x in x-direction. Velocity profile (bold dotted line) in the bulk part of the liquid is linear but extrapolates to $v_{\mathrm{liq}}(z_{\mathrm{wall1}})>0$ at the lower wall and to $v_{\mathrm{liq}}(z_{\mathrm{wall2}})<v_x$ at the upper wall, resulting in slip lengths b_1 and b_2, respectively. (b) The outer boundary of the lower wall is at temperature T_1, and the outer boundary of the upper wall is at T_2. Temperature profiles within the solid walls and in the bulk of the liquid are linear (but with different slopes due to different thermal conductivities in the three phases). Near interfaces, the profile (bold dotted line) deviates from linearity and discontinuously changes. The extrapolations of the bulk liquid and solid linear temperature profiles give the equivalent lengths h_1 and h_2 at the two interfaces in the system.

hancement of thermal conductivity in nanofluids is much less than estimated considering only the volume fractions of the matrix and solid particles.

The main complication with the measurement of transport across the solid-liquid interface is that it is very sensitive to the microscopic details of the solid surface, such as roughness, contamination by impurities, and the presence of gas between solid surface and the adjacent liquid layer.[4] This is why, in the past few years, many conflicting experimental results were obtained for slip lengths of simple Newtonian liquids such as water, reporting slip or no slip in flows past smooth hydrophilic[13,14] or hydrophobic surfaces,[15,16] increase[15,17] and decrease[18] in slip with surface roughness, and large deviations in apparently similar systems due to the details of surface preparation.[4,19] Dependence on surface roughness has also been observed in thermal boundary resistance measurements.[2]

Nonequilibrium simulations, with velocity[5–8,20] or temperature difference[21,22] imposed on the solid walls containing the liquid, have provided important insights into the interface transport depending on solid-liquid interactions[5–8,21,22] and interface roughness.[20] The resulting velocity and temperature profiles permit direct determination of both characteristic lengths of interface transport and the average coefficients in layers parallel to the wall. However, rate dependence of transport coefficients is an issue of concern in such simulations. In order to obtain satisfactory statistics, the simulations used to investigate interface transport are performed under shear rates and temperature gradients that, although still considered small for the simulation purposes, are, in fact, huge when translated into real-life situations. It is likely that interfaces will exhibit nonlinear response at values of the imposed gradient smaller than that requires to elicit the analogous nonlinear response for the bulk liquid. We expect this to be especially important in the case of the temperature gradient, where the local thermodynamic state (i.e., temperature) in different parts of the system is altered with the change of the temperature gradient.

The range of gradients in which the transport coefficients are gradient independent is clearly an important issue for nonequilibrium computer simulations and an important motivation for the development of a linear response theory for transport across interfaces. The linear response theory previously formulated by Barrat *et al.*[5,8,21] set out to derive Green–Kubo-type expressions for the slip and Kapitza lengths of a semi-infinite liquid against a planar solid surface. Elsewhere,[23] we have demonstrated that the slip length obtained from the expression in Ref. 5 was not an intrinsic property of the interface and suggested that the semi-infinite liquid presents a problem for linear response theory in relating the applied perturbation to the resulting gradient due to the inhomogeneity associated with the interface.

In this paper, we avoid the difficulties posed by applying homogeneous perturbations to heterogeneous phases. We do so by explicitly including boundary walls at which all perturbations are applied and whose fluctuations provide us with the desired linear response expressions for the transport of stress and heat through the contained phase, irrespective of how heterogeneous the latter is. As described in the following section, we can extract the related slip/equivalent lengths

by comparing the transport across a coexisting solid-liquid system with the transport through the bulk solid and liquid phases.

Here we first find slip and equivalent length for interfaces with different wetting characteristics by means of nonequilibrium simulations in several small gradients. Next, we use the boundary fluctuation method in the zero-gradient ensemble,[24,25] which directly provides the viscosity and thermal conductivity of the whole system. We extract the slip and equivalent length from the equilibrium results using the method described in Sec. II and compare them to the results of nonequilibrium simulations. In this way, we can determine if the small gradient results indeed represent the linear response, and in which wetting conditions are the nonlinear effects more important.

II. SLIP LENGTHS AND INTERFACIAL TRANSPORT COEFFICIENTS

In this section, we describe how to determine the quantities commonly used to describe the transverse momentum transport across interfaces, i.e., slip length b or Navier friction coefficient λ, and the corresponding heat flow coefficients, i.e., equivalent liquid length h, thermal boundary resistance R_K, and thermal conductance G_K from the transport coefficients across solid-liquid interface obtained using the BFT. We assume that the transport coefficients in each phase are equal to their bulk values, except in a narrow region close to the interface where they discontinuously change.

A. Shear flow past an interface

Let us consider a system consisting of a liquid of the thickness L_L, sheared between two solid walls, as illustrated in Fig. 1. The shear stress applied at the outer boundaries is σ. In the steady state, shear stress is constant and independent of position going from the solid walls into the liquid. The upper wall moves with the velocity v_{wall} with respect to the lower wall (assumed at rest). Shear viscosity of the bulk liquid is η_L. From Fig. 1(a), the strain rate in the liquid is $\gamma_L = v_{\text{wall}}/(L_L + b_1 + b_2)$, where b_1 and b_2 are the slip lengths at the solid-liquid interfaces with the lower and upper walls, respectively, and the shear viscosity of the bulk liquid is

$$\eta_L = \frac{\sigma}{\gamma_L} = \frac{F_x/S}{v_{\text{wall}}/(L_L + b_1 + b_2)}. \tag{1}$$

In Eq. (1), F_x is the friction force at either of the interfaces (friction forces at two interfaces are of equal magnitude and opposite direction), and S is the area of the interface. For given thermodynamic conditions (e.g., pressure, temperature), slip lengths b_1 and b_2 are considered to be intrinsic properties of the two interfaces (their roughness and solid-liquid interactions) and independent of type of flow or flow geometry, such as liquid thickness.

Instead of using slip length, transport across each interface can be described by the Navier friction coefficient

$$\lambda = \frac{F_x/S}{v_{\text{wall}} - v_{\text{liq}}(z_{\text{wall}})}, \tag{2}$$

where $v_{\text{liq}}(z_{\text{wall}})$ is the streaming velocity profile in the liquid extrapolated to the interface. Like slip length, the Navier friction coefficient is an intrinsic property of each interface, inversely proportional to slip length [Fig. 1(a)]

$$\lambda_{1,2} = \eta_L / b_{1,2}. \tag{3}$$

BFT in the zero-gradient ensemble[25] gives access to an *empirical* friction coefficient μ,[23] which is defined as the ratio of shear stress measured at two planes and their relative velocity. If the planes are chosen inside the solid walls, e.g., the outer solid planes separated by $L = L_L + L_{S1} + L_{S2}$ in Fig. 1(a), then the empirical friction coefficient can be related to the intrinsic slip lengths by

$$\mu = \frac{F_x/S}{v_{\text{wall}}} = \frac{\eta_L}{L_L + b_1 + b_2}, \tag{4}$$

independent of solid thicknesses $L_{S1} + L_{S2}$. In contrast to slip length b and the Navier friction coefficient λ, the friction coefficient μ is not an intrinsic property of an interface. μ is size dependent and decreases with L_L, the thickness of the liquid. The decrease of μ with L_L reflects the fact that shear stress decreases with the decrease in strain rate. If we move two walls at different wall separations with the same relative velocity, the strain rate at the larger separation will be lower, which will result in lower shear stress in the larger system.

BFT expresses μ in terms of the force autocorrelation integral,

$$\mu = \frac{1}{S k_B T} \int_0^\infty \langle \Delta F_x(t) \Delta F_x(0) \rangle dt, \tag{5}$$

where $\Delta F_x = (F_{x1} - F_{x2})/2$, and F_{x1} and F_{x2} are the friction forces on wall 1 and wall 2, respectively. The right-hand side of Eq. (5) is obtained using linear response theory when the external perturbation is constant relative wall velocity, and describes the momentum transport across the whole system, rather than an individual interface. The force autocorrelation integral decreases with liquid thickness as given by Eq. (4), and only allows the evaluation of the sum of the two slip lengths.[23] Bocquet and Barrat[5] presented an expression similar to Eq. (5) except that they claimed that it was the intrinsic Navier friction λ. In Ref. 24, we have presented an extended demonstration that the right-hand side of Eq. (5) corresponds to the empirical friction coefficient μ.

B. Heat flow across an interface

Similar considerations apply to energy transport across a system heterogeneous in z-direction. If the outer boundaries of the system consisting of a liquid between solid walls are kept at different temperatures T_1 and T_2 [Fig. 1(b)], the energy flux J_Q will in steady state be constant across any plane parallel to the interfaces, and the temperature profile $T(z)$ will be linear within each phase, with discontinuities ΔT_1 and ΔT_2 at each solid-liquid interface. Heat transport across an interface is characterized in analogous way to interface friction. Equivalent length h at each interface is the distance

at which the liquid temperature profile extrapolates to the solid temperature at the interface [Fig. 1(b)], in analogy to slip length. Kapitza conductance, which is the ratio of the heat flux and the temperature discontinuity at the interface,

$$G_K = J_Q/\Delta T = \kappa_L/h, \tag{6}$$

is analogous to the Navier friction coefficient.

It is usually assumed that all of the "temperature slip" occurs on the liquid side of the interface. If we allow for the possibility that there is a narrow region of the solid near the interface with heat conducting properties influenced by the presence of the liquid [dotted line in Fig. 1(b)], then the linear profile in the solid should first be extrapolated to the interface. The equivalent length h found in this way will contain contributions from both liquid and solid.

The BFT of heat transport gives the ratio ζ of heat flux and temperature difference in terms of heat flux fluctuations,

$$\zeta = \frac{J_Q}{\Delta T} = \frac{S}{k_B T^2}\int_0^\infty \langle \Delta J_Q(t)\Delta J_Q(0)\rangle dt, \tag{7}$$

where $\Delta J_Q = J_{Q1} - J_{Q2}$ is the net heat flux through the two outer boundaries. If the temperatures T_1 and T_2 are maintained using the Nosé–Hoover thermostats, the heat flux ΔJ_Q can be expressed in terms of the Nosé–Hoover thermostat multipliers α_1 and α_2 in the thermostated layers,[24]

$$J_Q = \tfrac{3}{2}k_B(N_2\alpha_2 - N_1\alpha_1)/S = \tfrac{3}{2}k_B\Delta\alpha/S, \tag{8}$$

where $\Delta\alpha = N_2\alpha_2 - N_1\alpha_1$, and N_1, N_2 are the numbers of thermostated atoms in the thermostated solid and amorphous boundary layers, respectively. Using Eq. (8), we obtain the expression for ζ in terms of fluctuations in the Nosé–Hoover multipliers,

$$\zeta = \frac{9k_B}{4ST^2}\int_0^\infty dt\langle \Delta\alpha(t)\Delta\alpha(0)\rangle. \tag{9}$$

The empirical thermal conductance ζ can be expressed in terms of thermal conductivities of the solid walls κ_{S1}, κ_{S2}, thermal conductivities of bulk liquid κ_L, and the equivalent lengths h_1, h_2 or Kapitza conductances, $G_{\kappa 1}$ and $G_{\kappa 2}$, of the two bounding interfaces,

$$\frac{1}{\zeta} = \frac{L_{S1}}{\kappa_{S1}} + \frac{L_L + h_1 + h_2}{\kappa_L} + \frac{L_{S2}}{\kappa_{S2}} = \frac{L_{S1}}{\kappa_{S1}} + \frac{1}{G_{K1}} + \frac{L_L}{\kappa_L} + \frac{1}{G_{K2}} + \frac{L_{S2}}{\kappa_{S2}}. \tag{10}$$

Like the empirical friction coefficient μ, the empirical heat transport coefficient ζ is explicitly size dependent. It depends on relative thicknesses of solid walls and liquid, and has a more complicated form than Eq. (4) because solid thermal conductivities are finite.

An expression similar to Eq. (7) (with heat flux evaluated at the interface instead of at the boundaries) has been previously[21] identified—wrongly, we argue—with the *intrinsic* Kapitza conductance G_κ [defined in Eq. (6)] instead of the *empirical* coefficient ζ. The heat flux autocorrelation integral, Eq. (7) or (9), reflects thermal conductivity of the system as a whole and can in principle give access only to the sum of equivalent lengths or a combination of Kapitza conductances on the two interfaces with bounding solid walls.

III. SIMULATION DETAILS

The empirical interface transport coefficients μ and ζ obtained in equilibrium simulations from Eqs. (5) and (9) contain transport properties across both interfaces. In order to obtain the intrinsic slip/equivalent length across a single interface, we attempted to isolate one liquid-solid interface by matching the structure of the system boundaries with the structure of the adjacent phase.[26] We have chosen this system because in our previous work[24,25] the influence of slip/equivalent length was negligible in the linear response limit, and we hoped to be able to neglect b_2 in Eq. (4) and h_2 in Eq. (10).

Our system consists of the Lennard–Jones (LJ) solid and liquid in coexistence, with different solid-liquid interaction parameters determining the wetting characteristics.

The parameters of the liquid-liquid interaction potential were the exclusion diameter $\sigma_L = 1$ and the depth of potential well $\varepsilon_L = 1$, i.e., the liquid-liquid interaction parameters defined the system of reduced units. In the solid, we chose the same diameter $\sigma_S = 1$ as in the liquid for simplicity, and the depth of potential well for the solid-solid interaction was $\varepsilon_S = 10$. This makes the reduced melting temperature of the solid phase an order of magnitude lower (in ε_L units) than the melting temperature of the liquid phase, which is, for example, comparable to the difference in melting temperatures of a metal and water.

The liquid-solid pair interaction potential was of the form[8,21]

$$U_{LS}(r) = 4\varepsilon_{LS}\left[\left(\frac{\sigma_{LS}}{r}\right)^{12} - a_w\left(\frac{\sigma_{LS}}{r}\right)^{6}\right], \tag{11}$$

with Lorenz–Berthelot rules for the cross-interaction parameters, $\varepsilon_{LS} = (\varepsilon_L\varepsilon_S)^{1/2} = 10^{1/2}$ and $\sigma_{LS} = \sigma_L + \sigma_S = 1$, and a variable wetting constant a_w, which determines how closely the liquid atoms are bound to the solid surface. In fact, the cross-interaction potential, Eq. (11), is equivalent to the LJ potential with the parameters $\sigma = \sigma_{LS}/a_w^{1/6}$ and $\varepsilon = \varepsilon_{LS}a_w^2$. The relationship of ε to ε_L determines if the liquid atoms are more strongly bound to liquid or to solid atoms. Roughly, if $\varepsilon > \varepsilon_L$ the liquid can be considered "wetting" and if $\varepsilon < \varepsilon_L$ the liquid is "partially wetting" the solid. We investigated the interface effects on the system viscosity and thermal conductivity for three values of the wetting constant, $a_w = 1.0$ (liquid atoms are more attracted to the solid than to the other liquid atoms); $a_w = 0.562$ ($\varepsilon = \varepsilon_{LS}a_w^2 = \varepsilon_L$ and the solid-liquid interaction is similar to liquid-liquid interaction, but there is a small gap between solid and liquid at the interface because $\sigma = \sigma_{LS}/a_w^{1/6} > \sigma_L$); and $a_w = 0.3$ (nonwetting case with liquid atoms more strongly bound to other liquid atoms than to the solid). The cutoff distance for the interactions was $2.5\sigma_L$ and $2.5\sigma_S$ for the solid-solid and liquid-liquid interactions, respectively, and 2.5σ for the solid-liquid interaction (the range of solid-liquid interaction increased with the decrease in the wetting constant).

The same[8,21] or similar[7] potentials have been used to vary the strength of solid-liquid interactions, but with solid atoms either immobile[8] or tethered to the lattice sites by harmonic springs[7,21] (and solid-solid interactions equal to liquid-liquid interactions). In our simulations, no tethering is required to stabilize the solid structure.

Our systems consisted of a liquid of one species and face-centered cubic (fcc) solid of a second, higher melting point, species in coexistence. The interface is parallel to the (100) plane of the crystal. The crystal plane separations parallel to the interface were 0.78σ. The reduced temperature of the system was $T=1.0$ and the reduced pressure was $P=2.5$. The bulk solid and liquid densities at this state point are $\rho_s=1.063$ and $\rho_L=0.841$, respectively. The shear viscosity of the bulk liquid is $\eta_L=2.6$ and the thermal conductivity of the bulk liquid is $\kappa_L=7.2$. The bulk solid thermal conductivity is $\kappa_S=404$.

We performed simulations in systems with two liquid thicknesses. The systems were periodic in the x- and y-directions, with periods $L_x=L_y=12.4\sigma$. The solid phase was in the lower part of the cell (from $z=0$). For all systems, the solid phase consisted of $N_S=1536$ atoms (16 crystal planes) and had the same thickness. In order to create the outer solid boundary, the atoms in the four lowest crystal planes were frozen, and the atoms in the fifth crystal plane from the bottom of the cell represented the solid boundary. The role of the frozen solid layer is to provide an environment for the solid boundary similar to that in the bulk and prevent the local changes in crystal plane separations. We defined the position of the interface as the average z-coordinate of the center of mass of the crystal plane adjacent to the liquid, and the solid thickness $L_S=5.45$ as the distance between the first mobile solid plane and the interface. These definitions are arbitrary to a degree (have an ambiguity of $\pm\sigma/2$), which reflects the ambiguity encountered in experiments.[3,4]

The larger system had the same z dimension of $L_z=28.4\sigma$ for all wetting constants. The number of liquid atoms was slightly larger for higher values of the wetting constant because of the increased liquid density close to the interface ($N_L=2425$ for $a_w=0.3$, $N_L=2480$ for $a_w=0.562$, and $N_L=2542$ for $a_w=1.0$). We determined the numbers of atoms in the liquid phase that result in the same pressure by trial and error: as wetting increased, we added atoms until the pressure was equal to 2.5 after equilibration.

For the boundary at the upper (liquid) end of the periodic cell, we froze the liquid atoms in the layer of thickness of 2.52σ. Each of the atoms in the layer of thickness 0.7σ below the frozen atoms was tethered to its current site with an anharmonic potential[24,25] of the form

$$U_{\mathrm{anh}}(\mathbf{r}_i) = -k_4[\mathbf{r}_i - \mathbf{r}_{\mathrm{eq}}(i)]^4 - k_6[\mathbf{r}_i - \mathbf{r}_{\mathrm{eq}}(i)]^6, \tag{12}$$

where $\mathbf{r}_i$ is the position of the ith tethered atom, $\mathbf{r}_{\mathrm{eq}}(i)$ is its equilibrium position, and the tethering constants have the values $k_4=5\times10^3$ and $k_6=5\times10^6$. The values were chosen so that the maximum displacement from the tethering site did not exceed 20% of the average distance between the nearest neighbors. The amorphous layer of frozen atoms and the tethered layer prevent the escape of liquid atoms out of the cell without disturbing the liquid structure next to the boundary.

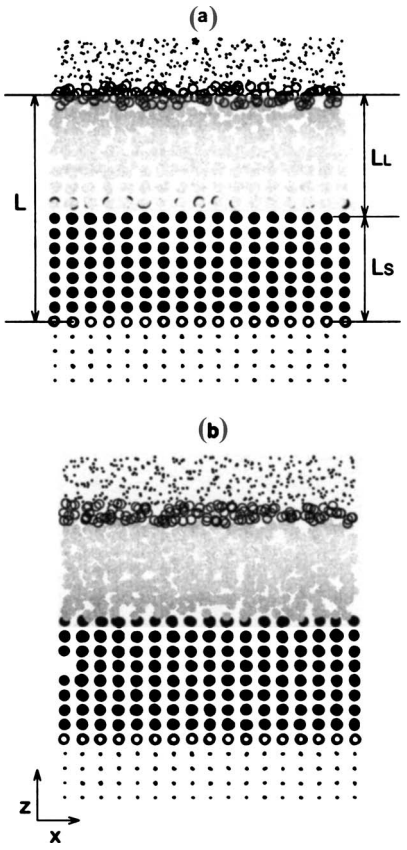

FIG. 2. Projection of the solid-liquid configurations for (a) $a_w=1.0$ and (b) $a_w=0.3$ for the smaller system used in equilibrium simulations onto the xz -plane. The immobile boundary atoms are shown as dots, the pinned thermostated layer of the liquid boundary atoms and the thermostated layer of solid atoms are shown as open circles, the freely moving liquid atoms are full gray circles, and the freely moving solid atoms are full black circles. The separation of the system boundaries is L, the liquid thickness is L_L, and the solid thickness is L_S.

In the smaller system we reduced the liquid thickness so that the new size of the whole system was $L_z=18.0\sigma$. The new liquid boundary was created from the larger configuration at the correct pressure by freezing a layer of atoms of the thickness $2.52\sigma_L$ on the outer edge and tethering the adjacent layer of atoms by the anharmonic potential. The pressure differences among all the systems were less than 0.1%.

The liquid thickness L_L appearing in Eqs. (4) and (10) was the distance between the center of mass of the thermostated tethered liquid atoms and the interface. The interface position again has the same uncertainty of $\pm\sigma/2$. In the larger system, L_L was equal to 15.6 and in the smaller system it was 5.20. The smaller configurations for $a_w=1.0$ and $a_w=0.3$ are plotted in Figs. 2(a) and 2(b), respectively.

The density profiles for the three wetting constants are shown in Fig. 3. The density profiles in the solid phase all show a small increase in separation between the crystal planes closer to the interface. The liquid structure close to the interface, in contrast, looks very different. For the highest value of the wetting constant, $a_w=1.0$, there are two layers of liquid atoms adsorbed to the solid surface at the solid density; this is partly due to our choice of the same liquid and

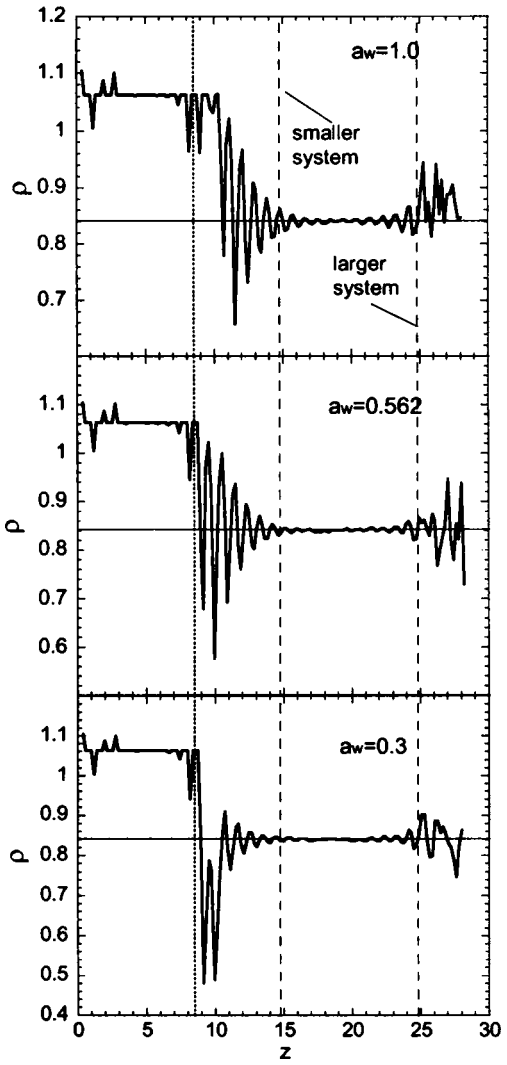

FIG. 3. Density profiles for the solid-liquid system with different wetting constants a_w [Eq. (14)]. The vertical dotted line shows the position of the interface. The full horizontal line shows the bulk liquid density $\rho=0.841$ at the pressure $P=2.5$. The dashed line shows the size of the smaller system used in equilibrium simulations.

solid molecular diameters. In the adjacent region, there is a high degree of layering parallel to the interface. The increased layering in the liquid structure at a lower density without adsorption is also present with the intermediate wetting constant $a_w=0.562$. At the lowest wetting $a_w=0.3$, the layering almost disappears, except for the appearance of a very low-density layer close to the interface. The apparent increase in structuring near the outer edge of the liquid is due to the density fluctuations in the frozen amorphous configuration. The same type of density fluctuations would be present in the bulk liquid at any time point, where they are not smoothed out in the averaging process.

In nonequilibrium shear simulations, the solid and amorphous boundaries move at a constant velocity v_{wall} with respect to each other, and the Nosé–Hoover thermostats act on the motion of solid atoms next to the frozen layer and on liquid atoms in the tethered layer. The liquid and solid atoms between the walls obey Newton's equations of motion. The applied shear rate is the relative wall velocity divided by the wall separation. We average the velocities in layers of thickness of 0.84 to find the average profile. Slip length b is obtained by interpolation of the linear velocity profiles far from the interface.

In the heat flow nonequilibrium simulations, the solid and liquid layers next to the immobile atoms are thermostated at different temperatures. The liquid and solid atoms in between obey Newton's equations of motion. We average the temperature profile in layers of thickness of 0.84. We determine the equivalent liquid length h by interpolation of the linear temperature profiles far from the interface region.

The zero shear rate ensemble is a system in which the frozen atoms and the tethering sites of the pinned liquid layer are not moved.[25] The zero temperature gradient ensemble is realized by applying the independent Nosé–Hoover thermostats with the same control temperature to the first free solid layer next to the frozen atoms,[23] and to the tethered liquid boundary layer (Fig. 2). The atoms enclosed between the boundaries do not have a thermostat[24] and move according to Newton's equations of motion.

All equations of motion were integrated using fifth order gear predictor-corrector scheme with the time step of 0.001 (in the liquid reduced units). The lengths of both nonequilibrium and equilibrium runs was 5×10^7 timesteps. The values of force or energy flux differences were recorded every four timesteps. The correlation functions were calculated using the shifting register technique[27] with a time window of 7500 records (or 30 000 timesteps). Each recorded value was used as an initial point for the averaging of the correlation function.

IV. SIMULATION RESULTS

A. Viscosity

The results of nonequilibrium shear flow simulations for the larger system ($L_L=15.6$) are presented in Figs. 4(a)–4(c). We calculated the flow velocity profiles for two relative wall velocities, $v_{\text{wall}}=0.078$ (corresponding to the average shear rate between walls $\gamma_{\text{wall}}=v_{\text{wall}}/L_L=0.005$, full circles) and $v_{\text{wall}}=0.156$ ($\gamma_{\text{wall}}=0.01$, open circles). The full vertical line is the position of the interface. For the lower shear rate, we did not observe shear heating in any of the studied systems, while for the higher shear rate the largest deviation from $T=1.0$ was $\sim2\%$. Since shear heating is a second order effect in shear rate, we expect linear response theory to be valid for the two shear rates we used. Note that these "very small" strain rates are still huge in experimental terms; our lowest strain rate of 0.005 would translate to $\sim10^{13}$ s^{-1} in the case of argon.

The slip lengths obtained by extrapolation of the velocity profiles for the two shear rates are the same, meaning that the response is, indeed, linear (i.e., rate independent). In this simple system, the interfacial effects are very small; the magnitude of slip length b is of the order of molecular diameter and is positive only for the lowest value of the wetting constant. For the two larger wetting constants, the adsorbed atoms do not take part in shear flow and slip occurs within the liquid, so that the corresponding value of b is negative.

Since in the smaller system liquid density profile shows considerable layering throughout the liquid volume, we per-

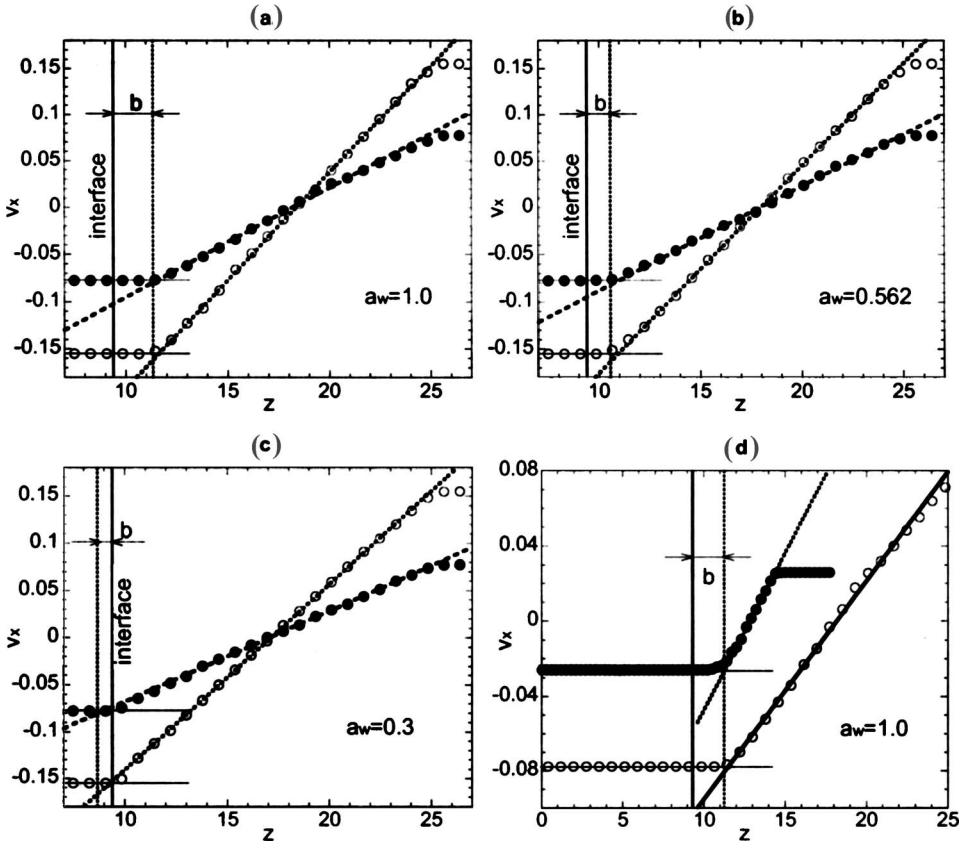

FIG. 4. Velocity profiles from nonequilibrium simulations of shear flow in the three solid-liquid systems. [(a)–(c)]. The full circles represent the profiles with the applied shear rate $\gamma = v_{\text{wall}}/L = 0.005$ and the open circles correspond to $\gamma = 0.01$. The full vertical line is the position of the interface and the dotted vertical line is the slip length b found from equilibrium simulations in the smaller system. In (d), we compare slip lengths found in the smaller (full circles) and larger systems (open circles) at similar applied shear rates $\gamma \approx 0.005$.

formed another set of simulations on a smaller system ($L_L = 5.2$) with relative wall velocity $v_{\text{wall}} = 0.026$ in order to check for the size dependence of slip length used in equilibrium simulations. The result for the two sizes at $a_w = 1.0$ (the highest degree of layering) in Fig. 4(d) shows that layering does not influence slip length at this system size. The results for the other wetting constants show similar agreement (see Table I). In all cases, the extrapolation was done using linear regression of the velocity profiles between the distance of two atomic diameters from the liquid-solid interface and the distance of one atomic diameter from the estimated interface of the liquid and the amorphous wall.

In addition, we found the slip length b from Eq. (4) (with $b_1 \equiv b$ and $b_2 = 0$) by direct measurement of the average force F_x exerted by liquid on the solid across the interface,

$$b = \frac{\eta_L}{\mu} - L_L = \frac{\eta_L v_{\text{wall}}}{F_x/S} - L_L. \tag{13}$$

The results are presented in Table I and are in good agreement with the extrapolation results. It is worth noting that the standard error in F_x is of the order of 0.5%, leading to the error in the first term of the order of 0.01. However, the uncertainty in the definition of the interface position is of the order of half the molecular diameter, leading to the uncertainty in L_L of at least the same order. This means that the largest uncertainty in the determination of slip length comes from the ambiguity in the definition of the interface position. This is true not only in simulations but also in experiments.[4]

These results agree with previous simulation results.[5–7] The main reasons why the effects are so small are that we

TABLE I. The intrinsic slip length b at the crystal-liquid interface as calculated from nonequilibrium and equilibrium simulations. The nonequilibrium value of b is obtained from the construction shown in Fig. 4. The equilibrium value of b is obtained using Eq. (13), assuming that the slip length at the amorphous wall is zero.

		Nonequilibrium			Equilibrium	
a_w	L_L	γ	F_x/S	b	μ	b
1.0	15.6	0.005	0.0151	−2.2	0.197	−2.4
		0.01	0.0298	−2.0		
	5.2	0.006	0.0253	−2.0	0.79	−1.9
0.562	15.6	0.005	0.0136	−0.7	0.181	−1.2
		0.01	0.0193	−1.1		
	5.2	0.006	0.0161	−1.0	0.619	−1.0
0.3	15.6	0.005	0.0125	0.6	0.164	0.3
		0.01	0.0255	0.3		
	5.2	0.006	0.0140	0.6	0.441	0.7

chose the same sizes for solid and liquid atoms,[28] and that the pressure is relatively high.[29] The fact that we used an unconstrained solid-liquid interface, instead of a frozen or harmonically tethered solid, may have also contributed to increased momentum transfer between liquid and solid.

In equilibrium simulations, we found the friction coefficient μ from the correlation integral Eq. (5), with F_{x1} the force across a plane inside the solid, acting on the immobile solid atoms and the first moving crystal plane [see Fig. 2(a)], and F_{x2} the force on tethered and immobile atoms in the amorphous layer.

We judged that the integral

$$\mu(t) = \frac{1}{Sk_BT}\int_0^t ds\langle \Delta F(s)\Delta F(0)\rangle \tag{14}$$

has reached its long-time limit by $t=15$ for $a_w=1.0$ and $a_w=0.562$, and at $t=30$ for $a_w=0.3$ (see Appendix). We estimated the average value of μ as the mean value of the integral over the time interval from $t=15$ to $t=30$. The corresponding equilibrium slip lengths b, evaluated from Eqs. (5) and (7), are shown in Table I and as dotted lines in Fig. 4. They are within error bars of nonequilibrium results.

The plateau (steady-state) value decreases with the increase in liquid thickness, in agreement with Eq. (4). The plateau values for the larger-size system are very small and close to each other for all wetting constants, and would be difficult to distinguish on the same plot (see also Table I). We were able to obtain consistent results for slip length b for both system sizes because we performed lengthy simulations that gave the plateau values with great accuracy (standard error in the tail of the correlation integral was less than 1%)—the simulations that were very costly in terms of computer time for the larger system. The fact that slip lengths obtained in equilibrium and nonequilibrium simulations for two system sizes are consistent [see Fig. 4(d) and Table I] means that the smaller system is still suitable for determination of slip length despite the layering in the density profile; transverse momentum transport seems not to be affected by the molecular layering more than one to two molecular diameters away from the interface, at least for this simple system at this pressure and temperature.

B. Thermal conductivity

For the nonequilibrium thermal conductivity simulations, we generated a temperature gradient by setting the control temperatures in the NoséNHoover wall thermostats to $T_1=1.0-\Delta T/2$ at the solid end (i.e., the thermostated solid plane in Fig. 2) and $T_2=1.0+\Delta T/2$ at the amorphous end (thermostated tethered liquid layer in Fig. 2) in the solid-liquid systems of the two sizes described in Sec. III. The separation between the thermostated layers was $L=L_S+L_L \approx 20$ in the larger system, and $L\approx 10.6$ in the smaller system. In the determination of the thermal boundary resistances, the positions of the interfaces are again the largest, but unavoidable, source of error. In the larger system, we used the temperature differences of $\Delta T=0.02$ and $\Delta T=0.05$, which correspond to the overall temperature gradients $\Delta T/L\approx 0.001$ and $\Delta T/L\approx 0.0025$, respectively. In the smaller system, the temperature difference was $\Delta T=0.01$, roughly corresponding to the lower overall gradient in the larger system. Although small in the context of nonequilibrium simulations, these gradients would be huge when translated into real-life situations. For example, in the case of argon the lowest gradient used here would be $\Delta T=3.5\times 10^8$ K/m. In addition to the steady-state temperature profile, in each system we also monitored the average heat flux J_Q [calculated from the Nosé–Hoover thermostat multipliers as given by Eq. (8)] generated in the applied temperature gradient.

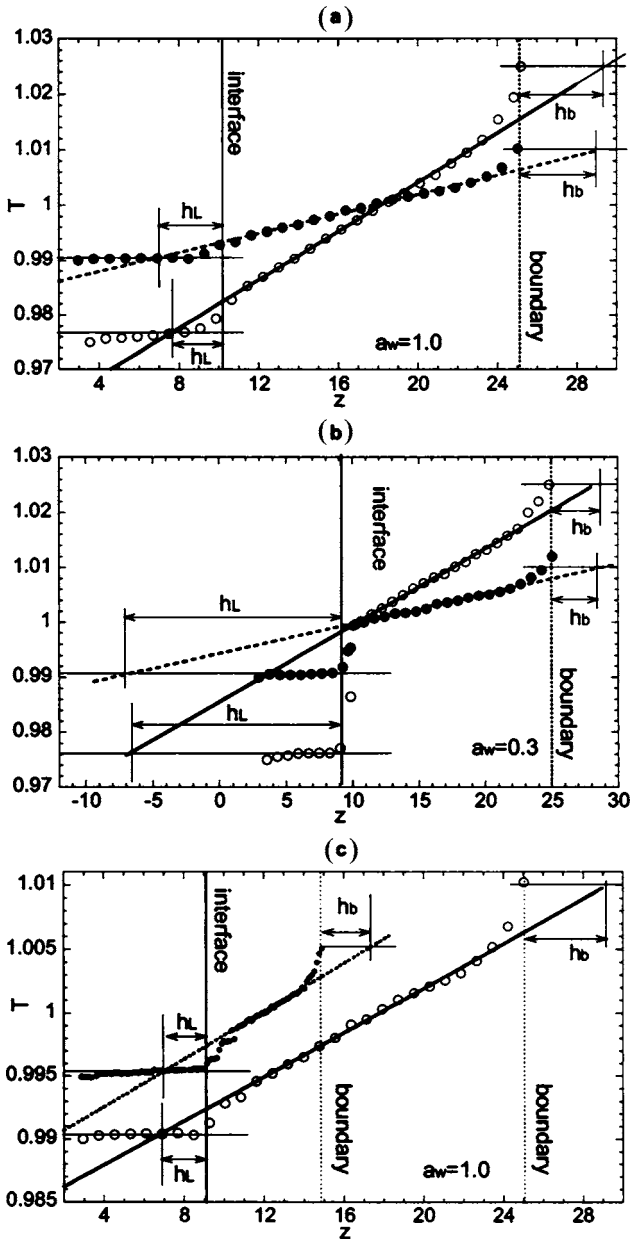

FIG. 5. Temperature profiles in two solid-liquid systems in temperature gradient. In (a) and (b), the full circles represent the profiles with the applied temperature gradient $\Delta T/L\approx 0.001$ and the open circles correspond to $\Delta T/L\approx 0.0025$. In (c), the full circles belong to the temperature profile in the smaller system, and the open circles to the larger system. The full vertical line is the position of the solid-liquid interface and the dotted vertical line is the position of the thermostat at the liquid end.

The temperature profiles for the two gradients and two system sizes are plotted in Fig. 5. We can see that in all cases

TABLE II. The intrinsic equivalent length h_L at the crystal-liquid interface and the sum h_L+h_b of the equivalent lengths from both interfaces calculated from nonequilibrium and equilibrium simulations.

			Nonequilibrium (from Fig. 5)		Nonequilibrium [from Eq. (15)]		Equilibrium [from Eq. (10)]	
a_w	L_L	ΔT	h_L	h_L+h_b	$J_Q\times10^3$	h_L+h_b	ζ	h_L+h_b
1.0	5.2	0.01	2.1	4.9	6.55	5.8	0.605	6.3
	15.6	0.02	2.1	5.8	6.61	6.1	0.333	5.9
		0.05	1.7	5.8	16.7	5.8		
0.562	5.2	0.01	7.5	10.8	4.65	10.2	0.468	10.1
	15.6	0.02	7.3	10.7	5.52	10.4	0.275	10.5
		0.05	5.7	9.9	14.0	10.1		
0.3	5.2	0.01	17.0	20.0	2.82	20.2	0.277	20.7
	15.6	0.02	16.5	19.9	4.07	19.7	0.201	20.1
		0.05	15.8	19.5	10.1	19.8		

there is a "bulk region" where the temperature profile is linear, implying that thermal conductivity is constant in this region. We assume that it does not greatly differ from bulk thermal conductivity κ_L at $T=1.0$, despite a slight deviation in temperature from $T=1.0$ in this region.

The equivalent length is always positive, i.e., there is always a thermal resistance between solid and liquid independent of wetting. The results show that an interface always causes a decrease in thermal conductivity, i.e., acts as an obstacle to energy flow, even when there is an adsorbed liquid layer of increased density. In the three simple systems we studied, the interface had a much larger effect on thermal conductivity than on viscosity. Interestingly, the nonlinearity in the temperature profile at the interfaces occurs on different sides of the interface, depending on whether the surface is low or high wetting. For the case of low wetting [Fig. 5(b)], the deviation from linearity in the temperature profile occurs on the liquid side of the interface [Fig. 5(b)], while in the high wetting case, this nonlinearity occurs on the solid side [Fig. 5(a)].

In some nanofluids, thermal conductivity is larger than purely expected from the solid and liquid volume fractions.[2] One proposed explanation is that there is an adsorbed liquid layer around the solid particles, and that this interface layer has thermal conductivity higher than the liquid. The results reported here, however, indicate that adsorbed layers do not produce the proposed enhanced conductivity. It is true, however, that thermal resistance increases with the decrease in solid-liquid interactions.

Unlike the case under shear, changing ΔT, the temperature offset of each interface changes both the temperature gradient between the two interfaces and the temperature at the interface. So, while both interfaces experience the same temperature gradient, they have different temperatures, one $+\Delta T$ and the other $-\Delta T$ from the temperature in the middle of the liquid (see Fig. 5). We expect the intrinsic equivalent length to linearly vary with the local temperature change ΔT for sufficiently small changes in temperature. If the two interfaces are identical, then this contribution should cancel out when we consider the sum of the equivalent lengths, while any influence due to the gradient would not cancel out. We do not have identical surfaces and so some dependence of h_L+h_b on the temperature difference of the two interfaces would be expected. In Table II, we also provide the results from nonequilibrium simulations where the equivalence lengths have been obtained, either directly from the graphical constructions such as shown in Fig. 5 or through the use of the following relation:

$$h = h_L + h_b = \left(\frac{\Delta T}{J_Q} - \frac{L_S}{\kappa_S}\right)\kappa_L - L_L. \tag{15}$$

The fact that we do not see any significant difference between the values of h_L+h_b calculated from the equilibrium and nonequilibrium simulations indicates that neither of these instrinsic equivalent lengths is exhibiting a dependence on the temperature gradient, i.e., the nonequilibrium simulations are probing the linear response region. This, in turn, means that whatever dependence of h_L on ΔT that we *do* see must be a result of the temperature dependence of the interfacial thermal resistance. We find that the equivalent length decreases, and hence the Kapitza conductance G_K increases, as the interfacial temperature drops. This temperature dependence has the same sign as that of the bulk liquid thermal

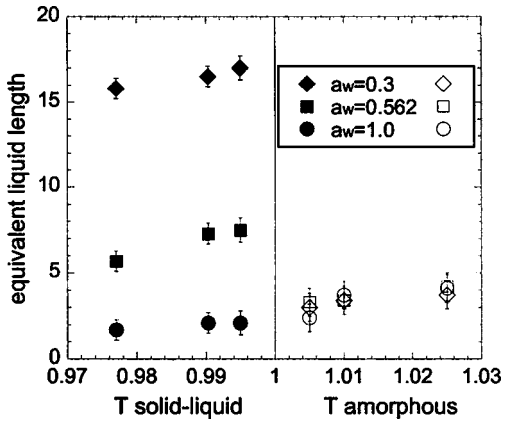

FIG. 6. (a) Dependence of equivalent liquid length on the temperature of the interface. Full symbols, equivalent length at the solid-liquid interface; open symbols, at the amorphous boundary. (b) The total equivalent liquid length h as a function of temperature difference ΔT between the system boundaries.

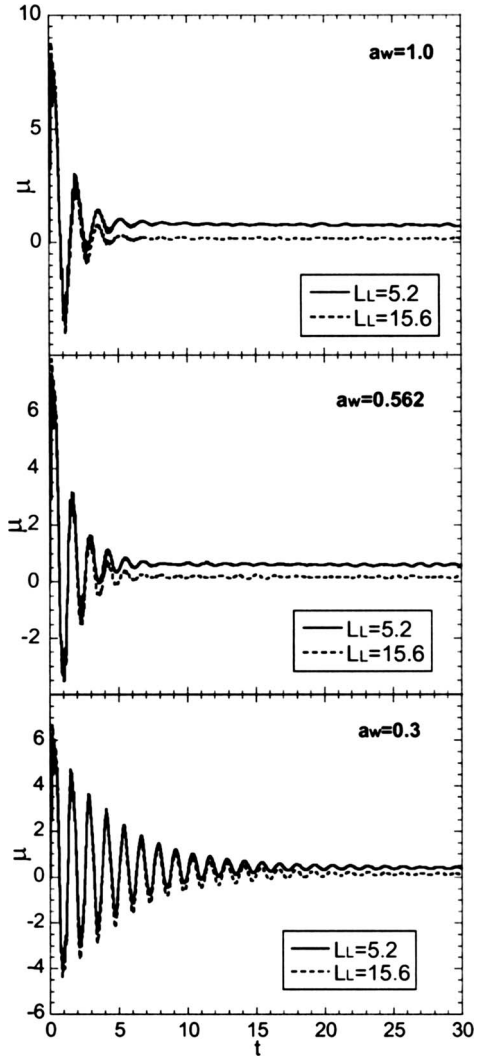

FIG. 7. Force autocorrelation integrals, Eq. (14), of three solid-liquid systems as the function of the upper time limit. Full line is the result for the smaller system, and the dashed line corresponds to the larger system.

conductance but the size of the temperature derivative of the interfacial conductance is larger than that of the bulk liquid.

The increase in equivalent liquid length with the increase in temperature for three wetting constants is shown in Fig. 6 (solid symbols). The effect of interface temperature (i.e., temperature of the last solid plane adjacent to the liquid) on the heat transport across the interface is much stronger than the effect of temperature change on thermal conductivity of the bulk liquid. The large change in thermal conductivity of nanofluids with the change in temperature[2] may be due to the same sensitivity to temperature of the heat transport close to the interface.

V. CONCLUSION

We have calculated the slip length and equivalent liquid length of the solid-liquid interface layer for three systems with different wetting properties at the same pressure and temperature using nonequilibrium methods, and compared them to the results of the equilibrium BFT. In agreement with previous simulation results,[21] slip length was positive for partial wetting and negative for large values of the wetting constant, where slip occurred within the liquid phase. For all values of the wetting constant, we could access the small strain rates required for linear response in nonequilibrium simulations.

We have found that, irrespective of wetting, the existence of an interface always decreased thermal conductivity relative to that of either the solid or the liquid, and the decrease was much larger when wetting was low.

Nonequilibrium simulations under low temperature gradient showed that there was a non-negligible thermal resistance both at the solid-liquid interface and at the interface between liquid and the amorphous wall with structure matching the liquid structure. Both thermal resistances (and the corresponding two equivalent liquid lengths) decreased with the decrease in the interface temperature. The decrease in thermal resistance with decrease in temperature is characteristic of the bulk behavior of LJ systems, but the temperature dependence appears to be stronger at interfaces. The sum of equivalent lengths was almost independent of the temperature difference at the external boundaries in the nonequilibrium calculations. While such independence would typically be taken as indicating linear response, the situation is not so simple in the case of thermal gradients due to the different thermodynamic states of the two interfaces. It is possible, for example, to have a gradient dependence on the interfacial thermal resistance masked by the equilibrium changes in the interfaces arising from changes to the interfacial temperatures. The near equality of the sum of two equivalent lengths as calculated from equilibrium and nonequilibrium simulations, however, provides strong evidence that the equivalent lengths are independent of the gradient and, hence, that the nonequilibrium calculations correspond to linear response.

ACKNOWLEDGMENTS

The authors would like to acknowledge the support of the Australian Research Council through the Discovery program. A generous grant of computer time from the Australian Partnership for Advanced Computing is gratefully appreciated.

APPENDIX: THE CONVERGENCE OF THE CORRELATION INTEGRALS EQUATIONS (17) AND (19)

The equilibrium simulation results for the friction coefficient μ in the solid-liquid systems with three types of wetting and two liquid thicknesses are presented in Fig. 7. We show the values of the correlation integral, Eq. (17), as a function of the upper time limit t. After long times ($t \to \infty$), the integral converges to a plateau value representing the friction coefficient μ.

At times shorter than the convergence times, it represents the form that the evolution of shear stress, measured as the average of the forces (per unit area) opposing the motion at both boundaries, would have if the frozen parts of the walls started to move in opposite directions with (small) constant velocities $\pm v_{\text{wall}}/2$ at $t=0$ (as a step function of time). Figures 7(a)–7(c) show that, when we start to slide a solid past a liquid at a constant velocity, we initially observe os-

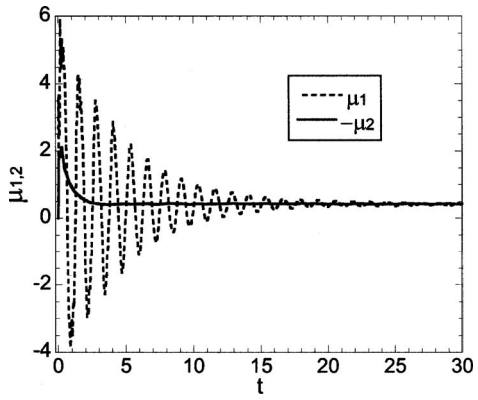

FIG. 8. Equilibrium result for the time dependence of the force on each of the walls, Eq. (A1). Force on the plane within the solid (dashed line) shows phonon oscillations, while force on the amorphous boundary is smooth.

cillations in the force needed to execute this motion. Damping of these oscillations is stronger if the wetting constant a_w is larger.

Figure 8 shows the forms of the transient forces in the smaller system on each of the frozen walls separately, i.e., it shows the correlation integrals

$$\mu_{1,2}(t) = \lim_{v_{\text{wall}} \to 0} \frac{F_{x1,2}(t)/S}{v_{\text{wall}}} = \frac{1}{Sk_BT} \int_0^t ds \langle F_{x1,2}(s) \Delta F_x(0) \rangle$$

for the lowest wetting constant $a_w = 0.3$ where the oscillations are the longest lived. Although the two forces have the same magnitude in the long-time limit, they differently behave in the transient period. Only the force across the plane inside the solid (force on the fixed outer atoms of the solid wall) shows oscillations (dashed line in Fig. 8). These damped oscillations are the result of the transverse elastic waves (phonons) in the solid, damped by the flow of the liquid past the interface. Without the interface with the liquid, the lifetime of the oscillations would be much longer. The attenuation of the collective solid motion is stronger if the liquid-solid coupling is stronger, i.e., if the wetting constant is larger. The force on the frozen liquid boundary does not oscillate (full line in Fig. 8), meaning that the transverse phonons originating in the solid do not propagate through the liquid.

The initial amplitude of oscillations increases with the liquid thickness and is related to the propagation of the initial shear stress needed to start shearing the system at a constant relative wall velocity at $t=0$. In order to start shearing a system with more liquid at the same constant strain rate, one needs to initially apply a larger shear stress, which then relaxes to a value determined by the system viscosity $\bar{\eta}$ as it propagates through the system. The lifetime of oscillations does not depend on the quantity of the liquid, but increases with the solid thickness for a given wetting constant.

In Fig. 9, we show the equilibrium simulation results for thermal conductivity of the three solid-liquid systems, i.e., the values of the correlation integral of the energy flux between the boundaries. The integral, Eq. (16), describes the linear response relaxation of heat flux if a constant temperature difference is imposed at the boundaries at $t=0$. There is very little difference in the general shape of the running cor-

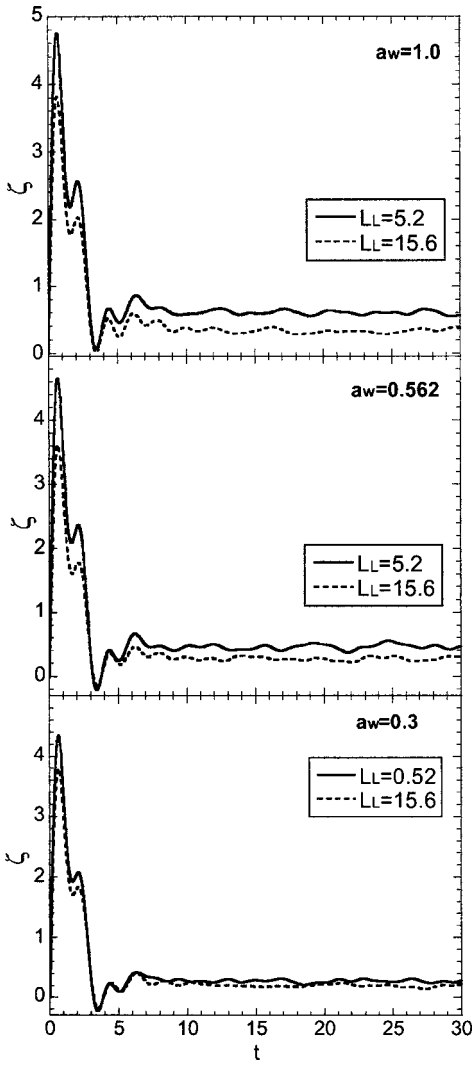

FIG. 9. Heat flux autocorrelation integrals, Eq. (16), of three solid-liquid systems as the function of the upper time limit. Full line is the result for the smaller system, and the dashed line corresponds to the larger system.

relation integrals in the systems with different liquid-solid interactions. At short times, there is a peak associated with the initial increase of the heat flux at the boundaries before the final temperature profile is established. The ensuing minimum is the result of the phonon reflection at the interface. The reflection is stronger for lower wetting where this minimum is more negative. There is much less oscillatory structure in the heat flux autocorrelation integrals than in the shear stress correlations.

The plateau value of $\zeta(t)$ is equal to

$$\zeta = \left(\frac{h + L_L}{\kappa_L} + \frac{L_S}{\kappa_S} \right)^{-1} \approx \frac{\kappa_L}{h + L_L},$$

where h is the sum of equivalent liquid lengths on all interfaces (in this case h_L at the solid-liquid interface and h_b at the interface between liquid and the amorphous wall). With the weaker wetting, h_L decreases while h_b remains unchanged, so that in the systems of the same sizes the plateau of ζ decreases with the decrease in wetting. In the systems with two same interfaces and different liquid thicknesses L_L, the plateau is lower when L_L is larger. However, for large

$h(h > L_L)$, as for $a_w = 0.3$ [Fig. 9(c)], the dependence of ζ on L_L becomes weak. This happens when the total thermal resistance at the two interfaces is larger than the total thermal resistance of the liquid in between ($\Sigma R_K > L_L/\kappa_L$), and the thermal conductivity of the whole liquid-solid system is largely determined by the interface resistance.

[1] P. G. de Gennes, Rev. Mod. Phys. **57**, 827 (1985).
[2] J. A. Eastman, S. R. Phillpot, S. U. S. Choi, and P. Keblinski, Annu. Rev. Mater. Res. **34**, 209 (2004).
[3] O. I. Vinogradova, Langmuir **11**, 2213 (1995).
[4] C. Cottin-Bizonne, B. Cross, A. Steinberger, and E. Charlaix, Phys. Rev. Lett. **94**, 056102 (2005).
[5] J.-L. Barrat and L. Bocquet, Phys. Rev. E **49**, 3079 (1994).
[6] P. A. Thompson and S. Troian, Nature (London) **389**, 360 (1997).
[7] P. A. Thompson and M. O. Robbins, Phys. Rev. A **41**, 6830 (1990).
[8] J.-L. Barrat and L. Bocquet, Phys. Rev. Lett. **82**, 4671 (1999).
[9] P. L. Kapitza, J. Phys. (USSR) **4**, 181 (1941).
[10] E. T. Swartz and R. O. Pohl, Rev. Mod. Phys. **61**, 605 (1989).
[11] O. M. Wilson, X. Hu, D. G. Cahill, and P. V. Braun, Phys. Rev. B **66**, 224301 (2003).
[12] S. T. Huxtable, D. G. Cahill, S. Shenogin, L. Xue, R. Ozisik, P. Barone, M. Usrey, M. S. Strano, G. Siddons, M. Shim, and P. Keblinski, Nat. Mater. **2**, 731 (2003).
[13] W. J. Huisman, J. F. Peters, M. J. Zwanenburg, S. A. de Vries, T. E. Derry, D. Abernathy, and J. F. van der Veen, Nature (London) **390**, 379 (1997).
[14] T. Becker and F. Mugele, Phys. Rev. Lett. **91**, 166104 (2003).
[15] E. Bonaccurso, H.-J. Butt, and V. S. J. Craig, Phys. Rev. Lett. **90**, 144501 (2003).
[16] Y. Zhu and S. Granick, Phys. Rev. Lett. **87**, 096105 (2001).
[17] V. S. J. Craig, C. Neto, and D. R. M. Williams, Phys. Rev. Lett. **87**, 054504 (2001).
[18] Y. Zhu and S. Granick, Phys. Rev. Lett. **88**, 106102 (2002).
[19] Z. Lin and S. Granick, Langmuir **19**, 7061 (2003).
[20] J. Gao, W. Luedke, D. Gourdon, M. Ruths, J. N. Israelachvili, U. Landman, J. Phys. Chem. B **108**, 3410 (2004).
[21] J.-L. Barrat and F. Chiaruttini, Mol. Phys. **101**, 1605 (2003).
[22] L. Xue, P. Keblinski, S. R. Phillpot, S. U.-S. Coi, and J. A. Eastman, J. Chem. Phys. **118**, 337 (2003).
[23] J. Petravic and P. Harrowell, J. Chem. Phys. **127**, 174706 (2007).
[24] J. Petravic and P. Harrowell, Phys. Rev. E **71**, 061201 (2005).
[25] J. Petravic and P. Harrowell, J. Chem. Phys. **124**, 014103 (2006).
[26] S. Butler and P. Harrowell, Nature (London) **415**, 1008 (2002).
[27] M. P. Allen and D. J. Tildesley, *Computer Simulation of Liquids* (Clarendon, Oxford, 1987).
[28] J.-L. Barrat and L. Bocquet, Faraday Discuss. **112**, 119 (1999).
[29] D. A. Edwards, H. Brenner, and D. T. Wasan, *Interfacial Transport Processes and Rheology* (Butterworth-Heinemann, Boston, 1991).